The Biophysics of the Fish Lateral Line

Sietse M. van Netten and Matthew J. McHenry

Keywords Cupula • Flow sensing • Hair cells • Kinocilia • Micromechanics • Microphonic • Nanometer • Neurobiology • Neuromast • Stereocilia • Swimming

1 Introduction

A distinctive feature of fishes is their ability to sense water flow with two types of receptors, called neuromasts, which are the functional units of the peripheral lateral line system. The superficial neuromasts (SNs) possess mechanosensory hair cells and project from the skin into the water at the body's surface. This is similar to the flow-sensitive organs of amphibians (Kramer, 1933), cephalopods (Budelmann & Bleckmann, 1988), coelenterates (Watson & Hessinger, 1989), and other invertebrates (Budelmann, 1989). However, fish also possess canal neuromasts (CNs), which are recessed below the body's surface, within cranial bones and scales on the trunk (Fig. 1a; see also the chapter by Webb). This second type of receptor provides a fish with an additional stream of information and thereby contributes a second submodality to the lateral line system. This chapter describes how the two submodalities are sensitive to distinct features of a flow stimulus because of biophysical differences between SNs and CNs.

S.M. van Netten (✉)
Department of Artificial Intelligence and Cognitive Engineering, University of Groningen, Nijenborgh 9, 9747 Groningen, The Netherlands
e-mail: s.m.van.netten@rug.nl

M.J. McHenry
Department of Ecology and Evolutionary Biology, University of California, 321 Steinhaus Hall, Irvine, CA 92617, USA
e-mail: mmchenry@uci.edu

S. Coombs et al. (eds.), *The Lateral Line*, Springer Handbook of Auditory Research 48,
DOI 10.1007/2506_2013_14, © Springer Science+Business Media New York 2013,
Published online: 29 June 2013

1.1 The Morphology of Neuromasts

Much of the biophysical difference between SNs and CNs stems from their distinct morphology. Both types include hair cells in a cluster within a sensory epithelium, or macula, but a SN typically contains about 10 of these cells (Fig. 1b), which is many fewer than the hundreds, or sometimes thousands, of hair cells within a CN (Fig. 1c; Dijkgraaf, 1963). A hair cell transduces small deflections into changes in membrane potential with mechanically gated ion channels that are located within the hair bundle of the cell (Hudspeth, 1989). The hair bundle consists of a kinocilium and microvilli (often referred to as stereocilia) on the apical surface of the cell that extend into a gelatinous structure called the cupula. Although there are noteworthy exceptions (Coombs et al., 1988), the CN cupula is generally hemispherical with a diameter in the hundreds of microns (Fig. 1c). The much smaller SN cupula is bullet shaped and is around 10 μm in width and 50–100 μm in height (Fig. 1b). In either neuromast, the cupula serves to transmit hydrodynamic forces from the flow of water near the surface of the body to deflect the hair bundles and thereby generates a nervous response. In this respect, CNs and SNs are governed by similar biophysics.

1.2 The Sensitivity of Neuromasts

Differences between SNs and CNs are reflected in a variety of physiological measurements. The hair cells within a neuromast change their membrane potential as the cupula is deflected. These deflections can be measured with optical techniques (van Netten & Kroese, 1987) and the resulting changes in voltage can be monitored by extracellular microphonic recordings (Kuiper, 1956). Changes in the membrane potential are encoded as a train of action potentials transmitted along afferent neurons toward the central nervous system. The frequency of these action potentials may also be recorded to measure the physiological response to a flow stimulus (Görner, 1963; Kroese et al. 1978; Coombs & Janssen, 1989; Kroese & Schellart, 1992; see also the chapter by Chagnaud & Coombs). Therefore, cupular deflection, microphonic potentials, and afferent action potentials are responses that vary with the magnitude of a stimulus and the sensitivity of the neuromast.

The sensitivity of a receptor, such as a neuromast, may be defined as the ratio of response output to stimulus input. The stimulus for a neuromast is conventionally provided by an oscillating sphere placed at sufficient distance to be unaltered by the presence of the body. The stimulus at this proximity is consequently defined as the freestream flow (Fig. 1a). With this arrangement, the sensitivity of a neuromast may be defined as the ratio of the amplitude of a response variable to the amplitude of a stimulus variable. For example, the sensitivity of the hair cells to stimulus velocity may be calculated by dividing the amplitude of microphonic potentials by the

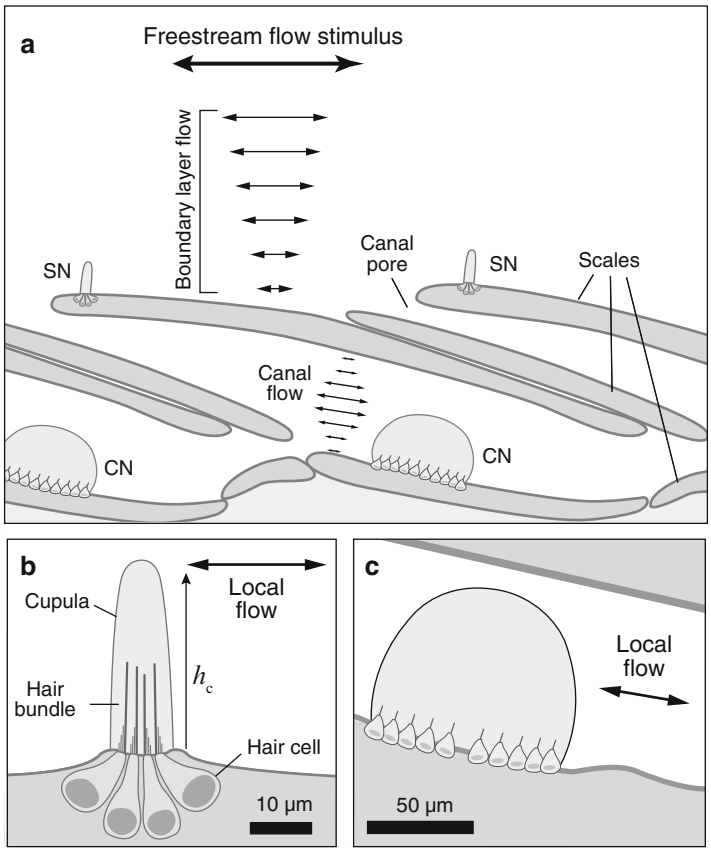

Fig. 1 The anatomy of lateral line neuromasts. Schematic illustrations show (**a**) the relative position and major anatomical features of (**b**) superficial and (**c**) canal neuromasts (Weber & Schiewe, 1976; Kroese & Schellart, 1992). (**a**) The superficial neuromasts extend into the water surrounding the body, where they are directly exposed to a flow stimulus. Canal neuromasts are enclosed in a channel that is formed of bone (on the head) or scales (on the trunk), where they encounter flow when a pressure difference exists between the pores that open the channel to the surface. Viscous hydrodynamics create a boundary layer at the surface and attenuate flow velocity within the canal and thereby filter a flow stimulus. (**b, c**) Neuromasts consist of mechanosensory hair cells, a gelatinous cupula, and support cells (not shown). The hair bundle of each hair cell extends into the cupula and thereby detects deflections of the cupular structure created by fluid forces. (**b**) The flow near the level of a cupula, local flow, may be defined at the height of the cupula for an SN (**b**) or the center of the canal for a CN (**c**)

amplitude of freestream velocity. The phase relationship between stimulus and response may also be encapsulated in this measure of sensitivity, as discussed in Sections 3.1 and 3.2.

The threshold sensitivity indicates the smallest stimulus that is required to create a response by a receptor. This limit of a receptor's performance depends on the strength of the response compared to the noise that is inherent to the receptor.

As discussed in Section 2.3, the transducer noise and Brownian motion are sources of noise in hair cells and have to be exceeded by a stimulus to produce a change in the firing rate of afferent neurons.

Sensitivity and threshold sensitivity have the potential to vary with the frequency of a stimulus. The frequency response indicates how sensitivity varies over a series of measurements over a range of stimulus frequency. The frequency response can be used to test whether a neuromast is sensitive to the velocity or acceleration of a flow stimulus. For example, sensitivity defined as the ratio of microphonic amplitude to velocity amplitude is predicted to remain constant across frequencies for a velocity-sensitive neuromast. In such a neuromast, microphonic potentials are in addition predicted to oscillate in phase with the freestream velocity. In contrast, the acceleration of freestream flow is phase-shifted by 90° and exhibits an amplitude that is proportional to frequency. Therefore, an acceleration-sensitive neuromast generates microphonic potentials that are phase-shifted by 90° with respect to freestream velocity. Such a neuromast would exhibit a sensitivity that is proportional to stimulus frequency, which is equivalent to a 20-dB increase per decade of frequency. As detailed in Section 2, such interpretations of frequency response measurements have supported the characterization of neuromasts as velocity (SN) and acceleration (CN) sensitive for a particular range of frequencies (Coombs & Janssen, 1989; Kroese & Schellart, 1992; see also the chapter by Chagnaud & Coombs).

2 Transfer Functions and the Frequency Response

The frequency response of a neuromast depends on how its hydrodynamics, structural dynamics, and neurophysiology vary with stimulus frequency. Each of these components may be modeled to examine their contribution to neuromast sensitivity. A model of a frequency response may be formulated as a transfer function [$H(f)$]. A transfer function is defined as the ratio of a response variable to a stimulus variable and therefore serves as a mathematical expression of sensitivity, as defined in Section 1.2. The transfer function generally uses complex notation that may be evaluated to yield the frequency response. In particular, the magnitude (i.e., absolute value) and argument of the transfer function respectively provide the amplitude and phase of the frequency response. For example, the hair bundle deflection generated by a velocity signal may be predicted (see Section 3.1) from a transfer function that is based on a biophysical model of cupular dynamics. Evaluating the magnitude and argument over a range of frequency values yields a prediction of the frequency response that may be compared with measurements from a physiological experiment. In the present context, a transfer function reveals how neuromasts filter different frequency components of a stimulus and offers a basis for understanding the salient differences between SNs and CNs.

2.1 Canal Neuromasts

Denton and Gray (1983, 1988, 1989) used a combination of physiological measurements with physical and mathematical modeling to study the biophysics of flow sensing in CNs. Their research on sprat examined the relationship between cupular deflection and the flow within the canal and how that flow varies in relation to freestream flow. These authors proposed that acceleration sensing emerges in the CN system due to dynamics at two levels. First, the velocity of flow within a canal is induced by pressure differences between its pores. Because a pressure gradient is proportional to the acceleration of freestream flow, the velocity within the canal is thus proportional to the temporal derivative of freestream velocity (Denton & Gray, 1983). Second, they proposed that a CN deflects with a displacement in proportion to the flow velocity within the canal owing to the viscous drag that acts upon the cupula. Therefore, the combined properties of the canal and CN cupula serve to encode the freestream acceleration of a flow stimulus.

Submicrometer measurements of cupular motion support this acceleration-sensing model for a restricted frequency range (van Netten, 2006). By measuring deflection in the CN at multiple positions within the cupula, it was revealed that the cupula slides as a rigid body along the surface of the sensory epithelium (van Netten & Kroese, 1987). These deflections are resisted by the spring-like hair bundles that anchor the cupula to the epithelium. A biophysical model of these dynamics predicts a constant cupular deflection per canal flow velocity across increases in frequency, up to about tens of Hertz in ruffe (*Gymnocephalus cernua*; Fig. 2d, green curve).

The hydrodynamics of the canal are also consistent with CN acceleration-sensing, as modeled with the hydrodynamics of a cylindrical channel (cf. van Netten, 2006). At low frequencies, the flow induced by a pressure gradient is governed by viscous interaction, known as Hagen–Poiseuille flow. The velocity of this flow adopts a parabolic profile with its most rapid flow in the center due to the viscous adhesion of water close to the channel wall (cf. van Netten, 2006). This condition has been modeled in general for channels (Sexl, 1930) and specifically for the lateral line (using a lumped parameter description; Denton & Gray, 1988). The model predicts that velocity within the canal is proportional to the acceleration of a freestream stimulus, which has been experimentally validated (Denton & Gray, 1983, 1988; Tsang, 1997). In accordance with this model, a transfer function of channel flow velocity per freestream acceleration is constant up to frequencies of tens of Hertz (Fig. 2c, green curve).

Mechanical filtering by the CN cupula and canal becomes more complicated at frequencies above tens of Hertz. The elasticity of the hair bundles causes the cupula to resonate, which creates an elevated ratio of cupular deflection to the canal flow velocity within the canal, known as the local velocity (Fig. 2d). The peak amplitude arises at a resonant frequency (~100 Hz), which depends on the stiffness provided by the hair cells and mass of the cupula and entrained water (van Netten, 1991). This is apparent in the almost hemispherically shaped cupulae of ruffe (van Netten

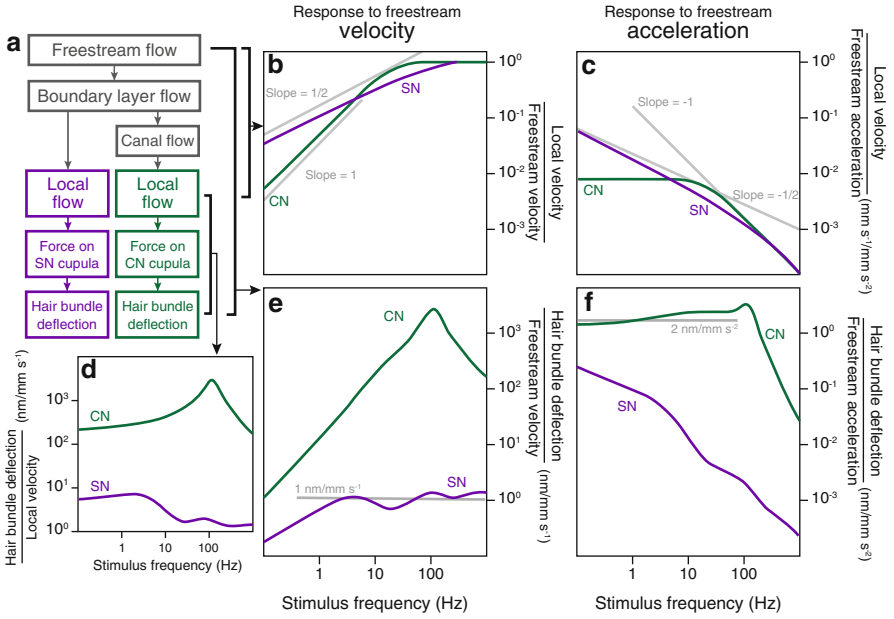

Fig. 2 The frequency responses of neuromasts. Transfer functions were used to model each component of the frequency response for the CNs (in green) and SNs (in purple) illustrated in Fig. 1. (**a**) A flow chart illustrates how these components alter a stimulus before it is encoded by the deflection of the hair bundles within a neuromast. This includes the boundary layer and canal flows (in gray) that alter the local flow that creates fluid forces that act on the cupula. (**b – f**) Each transfer function represents variation in a measure of sensitivity with the stimulus frequency. In this context, sensitivity is defined as a ratio of a response amplitude to a stimulus amplitude. In all plots, parameters for canal and CN transfer functions are taken from fits to measured cupular dynamics of ruffe (*Gymnocephalus cerua*) supraorbital canal neuromasts (van Netten, 2006). Parameters of SNs resulted from model-fits to measured cupular dynamics (Sendin et al., unpublished data.) for zebrafish (*Danio rerio*; McHenry et al., 2008). Lines of constant slope (in gray) are plotted for comparison. (**b, c**) The sensitivity of local velocity with respect to the velocity (**b**) and acceleration (**c**) of freestream flow. Local flow is defined at the location of the tip of the cupula for SNs and the center of the canal for CNs. These frequency responses are created for SNs by the boundary layer and for CNs by canal flows (Fig. 1). (**d**) The sensitivity of hair bundle deflection to local flow velocity depends on a fluid–structure interaction between the cupula, hair bundles and local flow. (**e**, **f**) These dynamics and the hydrodynamics of the boundary layer and canal combine to influence the sensitivity of the hair bundles to freestream flow. This overall sensitivity of the hair cells to a stimulus may be defined with respect to the velocity of freestream (**e**) or acceleration (**f**) of freestream flow. Constant overall sensitivity is indicated for SN of freestream (**e**) and CN (**f**) with a numerical value and a flat line (in gray) stretching across the appropriate frequency range

& Kroese, 1987) and the more elliptically shaped cupulae in the clown knife fish (Wiersinga-Post & van Netten, 2000). In the high-frequency range, the inertia of water causes flow in the canal to move in proportion to, and in phase with, the freestream stimulus. As a consequence, the amplitude of local canal velocity declines as stimulus frequency increases (Fig. 2c). The cutoff frequency that

marks this transition of canal filtering is inversely proportional to the square of the canal radius and therefore has the potential to vary with the body of a fish or between species (van Netten, 2006). This amounts to a cutoff frequency of approximately 20 Hz in ruffe, which have relatively large canals (Fig. 2c, green curve). This cutoff frequency is consequently predicted to be lower in the many species with smaller canals (see the chapter by Webb).

The flow signals detected by a CN depend on the combined filtering characteristics of both the cupula and canal. These composite properties may be examined by calculating the product of transfer functions, for the cupula and canal (i.e., Fig. 2c × Fig. 2d = Fig. 2f, green curves). In ruffe, the resonance peak created by the mass and stiffness of the cupula is somewhat higher than the cutoff frequency of the canal (~20 Hz). As a result, the attenuation in velocity created by canal hydrodynamics (Fig. 2c, green curve) at high frequency effectively removes the raise in sensitivity that is created by cupular resonance (Fig. 2d, green curve). This is also reflected in the frequency response of the discharge rate of afferent neurons (Wubbels, 1992), which can thus be mostly accounted for by the mechanical filtering of the canal and cupula. Additional electrical filtering by the hair cells exhibits a high-frequency cutoff that is close to the mechanical cutoff frequencies (Wiersinga-Post & van Netten, 2000). This may also explain the additional phase delay usually found in afferent responses (cf. Wubbels, 1992), as compared to accompanying phase delays (~ −180°) of the combined mechanical filtering at high frequencies.

2.2 *Superficial Neuromasts*

Deflection measurements of the cupulae in zebrafish (*Danio rerio*) suggest that SNs operate in a fundamentally different manner from CNs. The elongated cupula of a SN bends in flow (Dinklo, 2005), which is unlike the rigid-body motion of the CN (van Netten, 1988). The forces transmitted to the hair bundles in the SN thus also depend on the beam dynamics of the cupula, which vary with its material properties and dimensions (McHenry et al., 2008). This material is a compliant mucopolysaccaride gel (Young's modulus <100 Pa), which allows the cupula to bend with high flexibility (McHenry & van Netten, 2007). Although located at the surface of the body, a SN is exposed to hydrodynamic filtering that is similar to the filtering provided by the CN canal. As in the canal, water adheres to the surface of the skin and thereby creates a spatial velocity gradient, here called the boundary layer (Schlichting, 1979). The boundary layer and the fluid–structure interaction with the cupula provide two layers of mechanical filtering in the SN frequency response.

The role of the boundary layer in SN sensitivity may be modeled with hydrodynamic theory (Schlichting, 1979). This model is formulated as a transfer function that describes sensitivity of local velocity (at the height of the cupula, $h_c = 45$ μm; cf. Van Trump & McHenry, 2008) relative to the stimulus velocity in the freestream (Fig. 2b, purple curve). As detailed in the chapter by McHenry and Liao, the boundary layer may be characterized by the thickness from the body's surface at

which the flow velocity approximates freestream flow. In oscillatory flow, the boundary layer thickness decreases with frequency as inertial forces increasingly overcome viscosity and the flow velocity decreases near the surface. For low frequencies (<100 Hz), the velocity at the cupular height varies as a fractional (power of 0.5) time derivative of the freestream velocity (cf. Kalmijn, 1988), which is apparent from the 0.5 slope of the transfer function (i.e., 10 dB/decade, Fig. 2b, purple curve). This contrasts canal filtering (20 dB/decade, Fig. 2b, green curve), which provides a "full" derivative with respect to the freestream at low frequencies. At higher frequencies, the boundary layer thickness reduces to below the cupula height and, as a consequence, the SN cupula is acted upon by the full freestream stimulus. In this manner, the boundary layer functions as a high-pass filter with a cutoff frequency determined by the cupula height.

The mechanical filtering generated by the SN cupula has been considered by a mathematical model. By treating the cupula as a flexible beam in flow and modeling the forces generated by fluid motion, this model predicts the deflection of hair bundles for an oscillatory stimulus (McHenry et al., 2008). This model has been applied to the SN cupulae of zebrafish (*Danio rerio*) (Dinklo, 2005), which possess a morphology that is representative of SNs in many species of fish (Münz, 1989). A modified version of this model is presented here that incorporates new observations from experimental measures of cupula response using a micro fluid-jet stimulus (Sendin et al., unpublished data). This modified model predicts a nearly constant level of sensitivity to local flow (defined at $h_c = 45$ μm) for frequencies up to a few Hertz (Fig. 2d, purple curve). The exact cutoff frequency is determined by cupular dimensions (here both diameter and height), its material stiffness, as well as hair bundle stiffness. Beyond this cutoff, a slow decline in sensitivity is exhibited with increasing frequency.

The combined filtering provided by the cupula and boundary layer may be determined by the product of their transfer functions, which represents the sensitivity of hair bundle deflection to freestream stimulus velocity (Fig. 2b × Fig. 2d = Fig. 2e, purple curves). This result demonstrates that the SN hair bundles deflect in proportion to flow velocity, with high-pass filtering. However, it appears likely that the neurophysiology of the hair cells may attenuate signals at frequencies beyond tens of Hertz, as observed in several studies of afferent responses and extracellular receptor potentials (Kroese, 1978; Kroese & Schellart, 1992; Sendin et al., unpublished data).

2.3 Threshold Sensitivity

The frequency response can also provide a basis for estimating the threshold sensitivity of a neuromast, which is the minimum stimulus that may be detected. In the CN of ruffe, the constant acceleration-sensitivity below the cutoff frequency (~100 Hz) has an approximate value of 2 nm of hair bundle displacement

per mm s^{-2} of flow acceleration (Fig. 2f, green curve). The threshold sensitivity may be calculated as the acceleration necessary to deflect the hair cells to a degree equal to the noise that is inherent to mechanotransduction. In particular, the transducer noise and Brownian motion for the 1000 hair cells of ruffe are estimated to be 0.20 nm (root mean square). (cf. van Netten, 2006). For low frequencies, a comparable signal would be generated by a stimulus with an acceleration amplitude of about 0.10 mm s^{-2}. This estimate of threshold sensitivity for supraorbital canal neuromasts is on the same order of magnitude as reports of behavioral measurements for sensitivity. For example, the mottled sculpin (*Cottus bairdi*) responds to flow near the cranium with an acceleration of about 0.18 mm s^{-2} (−75 dB re 1 m s^{-2} ; Coombs & Janssen, 1990).

The different morphology of SNs creates a lower threshold sensitivity than CNs. Zebrafish SNs possess approximately 20 hair cells (Van Trump & McHenry, 2008), which suggests a noise level of 1.45 nm r.m.s. For frequencies greater than a few Hertz, the SN sensitivity to velocity is 1 nm hair bundle displacement per mm s^{-1} of stimulus velocity (Fig. 2e). This suggests that a velocity amplitude of 1.45 mm s^{-1} is sufficient to produce a threshold response. This value is less than, but not inconsistent with, measurements of the threshold from recordings of afferent neurons from the same species (7 mm s^{-1}; Liao, 2010).

The superior response of CNs over SNs is maintained over a broad spectrum of frequencies for the same freestream stimulus. For example, a 20-Hz oscillation with an acceleration amplitude of 100 mm s^{-2} creates an amplitude of velocity equal to 0.79 mm s^{-1}. This stimulus would create hair bundle deflections of 200 nm in the CN and 0.79 nm in SN. Therefore, the CN response is 1000 times greater than threshold, whereas the SN response is about half of its threshold. Such disparities in sensitivity are evident for both velocity (Fig. 2e) and acceleration stimuli (Fig. 2f). This result is mostly due to the much larger cupula and greater numbers of hair cells in CNs, as indicated by the responses to flow at the level of the cupula (Fig. 2d). For example, CNs are 50 times more sensitive than SNs in the frequency range up to a few Hertz for a velocity stimulus at the SN cupular tip (h_c = 45 μm). An even greater disparity is generated at higher frequencies (>10 Hz), where CN cupulae resonate and SN cupular responses decline. However, the boundary layer within the canal impedes local flow more than the boundary layer at the surface at low frequencies (<4 Hz), which causes the overall sensitivity values of CNs to approach that of SNs. Nevertheless, this phenomenon does not alter the general conclusion that CNs have a much higher response than SNs in the bandwidth considered (Figs. 2e, f).

3 Responses in the Time Domain

A transfer function gives a complete representation of a linear filter and may therefore be used to calculate how a neuromast responds to a flow stimulus in the time domain. This calculation follows a procedure that is commonly described in

textbooks on linear signal processing (e.g., Lathi, 1998). However, this approach is rarely employed to understand animal sensory systems, despite the insight that it offers by articulating the signals that are encoded by the peripheral nervous system.

Here a brief practical introduction on time-domain filtering is presented with an illustration of its applications to the lateral line system. These calculations require signal processing software (e.g., Matlab, Matcad, Igor, Origin, Octave, Labview) to determine the complex fast-Fourier transform (FFT) and an inverse fast-Fourier transform (IFFT). The FFT converts a signal that varies with time (i.e., defined in the time domain) into a series of complex numbers that vary with frequency (i.e., defined in the frequency domain). The absolute value and phase of these complex values constitute the spectrum of the signal in the frequency domain. It is in the frequency domain that the response of a sensor (e.g., an SN or CN) to a stimulus may be calculated. The result, a response signal, may then be determined for the time domain with IFFT. IFFT does the reverse of FFT by converting complex frequency-domain signals into time-domain signals, which are real numbers.

3.1 Calculating a Filtered Signal in the Time Domain

Determining the response of a sensor to a stimulus requires first converting a signal, y, from the time domain into the frequency domain. This signal must be recorded at a sufficiently high sample rate that the period between samples, ΔT, is much shorter than the duration of the most rapid events in the signal. The first step toward filtering y is to add a series of zeros at the beginning and end that are both equal in duration to the (finite) impulse response of the filter to be used, a procedure known as zero-padding. The zero-padded signal is then converted into the frequency domain ($y \rightarrow \text{FFT} \rightarrow Y$) to produce a spectrum, Y, that possesses the same number of samples, N, as in the time domain. The increment between frequency values for this spectrum, Δf, is determined by the sample period and total number of samples [$\Delta f = (N\Delta T)^{-1}$].

As explained in Section 2, the frequency response of a sensor indicates how it filters a stimulus, as dictated by its transfer function, H. Calculating the response of the sensor requires evaluating the transfer function for the same frequencies as those contained in the signal spectrum. This evaluation produces values, H_{eval}, that are calculated as follows:

$$\begin{aligned} H_{\text{eval}} &= H(n\,\Delta f), \text{ for } n \in (0,\ 1\ .\ .\ .N/2-1), \\ &= H^{*}((N-n)\,\Delta f), \text{ for } n \in (N/2\ .\ .\ .N-1), \end{aligned} \tag{1}$$

where n is a series of N integers. The first part of the this definition evaluates H_{eval} up to half the number of frequency values [$n \in (0, 1\ .\ .\ .N/2-1)$], so that the highest frequency represented is a single sample less than half of the sample rate

[i.e., $(N/2)\Delta f = (2\Delta T)^{-1}$]. The second part of the definition of H_{eval} is related to the negative frequencies, which are also required in complex notation. The values at these negative frequencies are equal to the complex conjugate of the transfer function at the corresponding positive frequencies [i.e., $H(-f) = H^*(f)$] and are a translated copy of the discrete values of H defined for $n \in (N/2 \ldots N-1)$. As a consequence, a plot of values at negative frequencies is a mirror image of the values at these positive frequencies.

Using the frequency-domain representations of both the stimulus and sensor allows for the final calculation to determine the response in the time domain. Within the frequency domain, the response, S, is calculated as the pairwise product of elements in Y and H_{eval}. This response spectrum is then converted back to the time domain ($S \rightarrow$IFFT$\rightarrow s$) to reveal the sensor's responses, s. These responses are equivalent to the discretized version of the stimulus signal, y, convolved with the impulse response h, as indicated by the following equation:

$$s = \int_{-\infty}^{t} y(t')h(t-t')dt' \tag{2}$$

3.2 The Response to a Simple Stimulus

Time-domain filtering may be demonstrated by its application in a simple example. Consider a dimensionless stimulus composed of two frequency components, defined by the following equation:

$$y = a_{\text{low}} \sin(2\pi f_{\text{low}} t) + a_{\text{high}} \sin(2\pi f_{\text{high}} t), \tag{3}$$

where f_{low} and f_{high} respectively define low (1 Hz) and high (100 Hz) frequency components with amplitude values of a_{low} (1.25) and a_{high} (0.75) for the signal y. A series of values such as a stimulus measurement may be determined by sampling this function during a time interval ($0\text{ s} < t < 2\text{ s}$, $N = 1024$; Fig. 3a). The spectrum of this stimulus (Y, found via FFT) reflects its major frequency components with peaks in amplitude at 1 Hz and 100 Hz (Fig. 3b).

To illustrate how two sensors may differ in their response to this stimulus, the responses to both a low-pass and high-pass first-order filter are now considered. Such sensors are described by the following transfer functions (Lathi, 1998):

$$H_{\text{low}} = 1/(1 + (f/f_c)i), \tag{4}$$

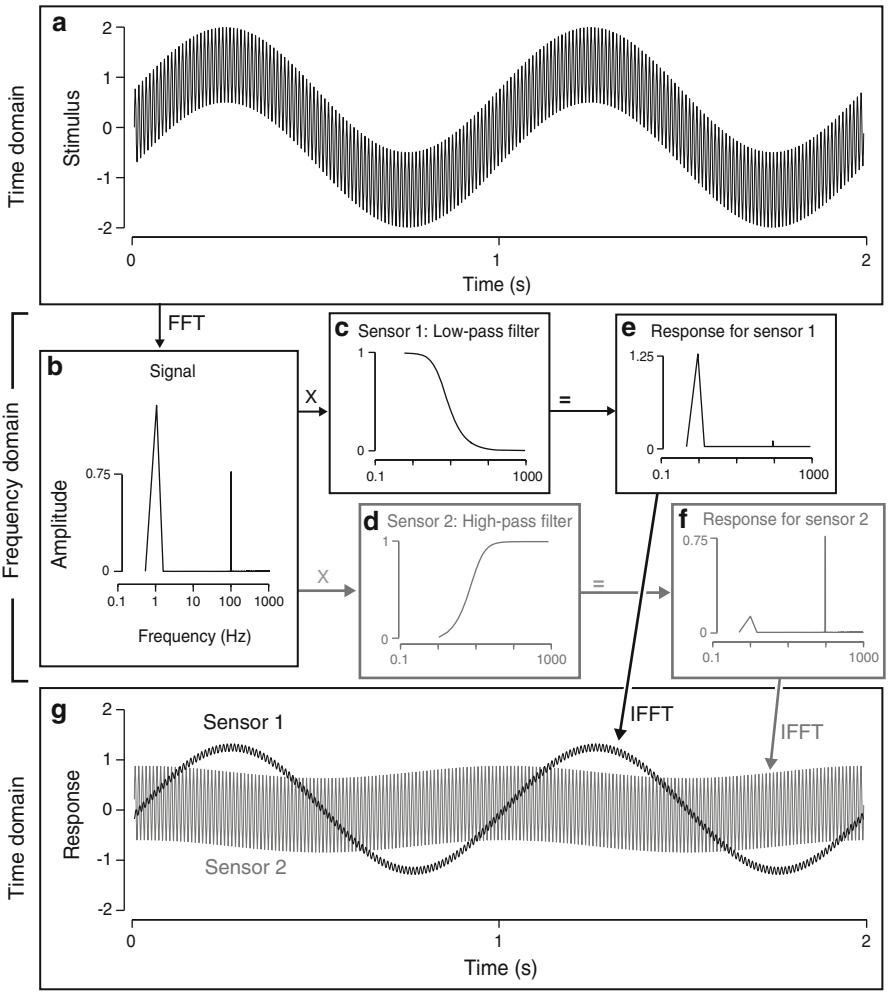

Fig. 3 Time-domain filtering employed to calculate the response of two sensors with distinct filtering characteristics. (**a**) For the purposes of illustration, the stimulus is modeled as a time-varying signal created by the sum of two sine functions (Eq. 1; see text for parameter values). This signal is converted from the time domain into (**b**) the frequency domain using a fast-Fourier transform (FFT). The resulting spectrum consists of a series of complex numbers for each frequency, the amplitude of which is shown. (**c**, **d**) In this example, the stimulus is detected by two sensors that possess distinct frequency response characteristics. (**c**) Sensor 1 is most sensitive to low frequencies and therefore functions as a low-pass filter. (**d**) In contrast, sensor 2 operates as a high-pass filter. (**e**, **f**) The response of both sensor 1 (**e**) and sensor 2 (**f**) is calculated in the frequency domain as the product of the signal spectrum (**b**) and the sensor spectra (**c, d**). These signals are then transformed into the time domain with IFFT. (**g**) The responses of sensor 1 (black) and sensor 2 (gray) demonstrate how the sensors respond differently to the same stimulus

$$H_{\text{high}} = 1 - (1/(1 + (f/f_c)i)), \tag{5}$$

where f_c is the cutoff frequency for each sensor ($f_c = 10$ Hz, in this example) and i denotes the (positive complex) root of -1 (Fig. 3c, d). These equations are evaluated to find their frequency responses. For example, the low-pass sensor maintains a relatively high-amplitude response to frequencies below the cutoff (Fig. 3c). Therefore, its response spectrum (Fig. 3e) maintains a high amplitude at 1 Hz, which is reflected in its response in the time domain (Fig. 3g). Conversely, the high-pass sensor attenuates the low-frequency components in favor of high frequencies that pass through to the response (Fig. d, f, g). These same steps may be employed to examine the differences between how SNs and CNs respond to a flow stimulus, based on their specific transfer functions.

3.3 The Responses to a Swimming Fish

The differences in frequency response between CNs and SNs are also reflected in their time-domain responses. An example is provided by a swimming goldfish (*Carassius auratus*; after Kalmijn, 1989). The displacement of the fluid increases on the approach of a neuromast (positive displacement in Fig. 4a) and subsequently passes zero (~0.25 s) before moving beyond the neuromast to produce a negative displacement. Most of the spectral power for this relatively slow stimulus signal is below 10 Hz, which is at the low end of the frequency range of the lateral line system (Fig. 2e, f).

The response of a SN to this stimulus (Fig. 4b, solid) was calculated with time-domain filtering (Section 3.1; cf. Fig. 3). This calculation used the transfer function to yield a displacement response for SN hair bundles (Fig. 2e, purple curve). This response appears to be almost identical in shape to the velocity of the stimulus (Fig. 4b, dashed line). This result illustrates how a SN can be considered a high-fidelity velocity detector for a low-frequency stimulus, even while the properties of a fractional time derivative of the boundary layer have been fully accounted for (cf. Goulet et al., 2012).

The CN response contrasts that of the SN for the same stimulus. The CN response (Fig. 4c, solid line) was calculated using time-domain filtering with the transfer function for the CN (Fig. 2f, green curve), applied to the stimulus acceleration (Fig. 4c, dashed line). The CN hair cell bundles sense a time waveform that closely follows the acceleration of the fluid flow. In addition, the CN hair bundles respond with a deflection that is about 50 times greater than in the SN (CN maximum ~1 μm vs. SN maximum ~20 nm; Fig. 4b, c), which is consistent with the differences in sensitivity interpreted from the frequency response (Section 2.3; Fig. 2d).

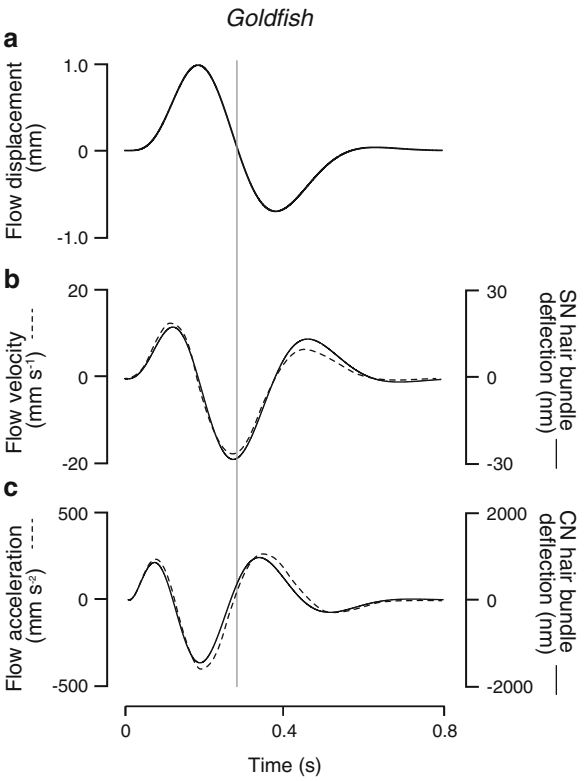

Fig. 4 Responses of SN and CN to a swimming goldfish calculated with time-domain filtering (Section 3.1; Fig. 3). (**a**) Freestream water displacement produced by a quietly approaching (positive going phase) and passing (negative going phase) goldfish (after Kalmijn, 1989; p. 204). (**b**) Hair cell displacement response of a SN (solid line) compared to the water velocity (dashed line) derived from the displacement shown in (**a**). (**c**) Hair cell displacement response of a CN (solid line) compared to the water acceleration (dashed line) derived from the displacement shown in (**a**). Parameters used for the transfer functions of SN and CN to calculate the filtered time responses were the same as used for Fig. 2. The vertical line indicates the time of passing by the neuromast ($t = 0.25$ s)

3.4 The Responses to Swimming Zooplankton

Biological flow stimuli can offer a broad range of frequency components, as illustrated by zooplankton that are detected by fish predators (Montgomery, 1989). For example, the crustaceans *Daphnia* and *Diaptomus* swim with appendages that create contrasting flow signals. *Daphnia* swimming is powered by a pair of antennae that propel the body in discrete pulses. *Diaptomus* use a series of swimmerets along the abdomen that operate with high frequency and low amplitude to move the body forward at a relatively steady rate. To examine how

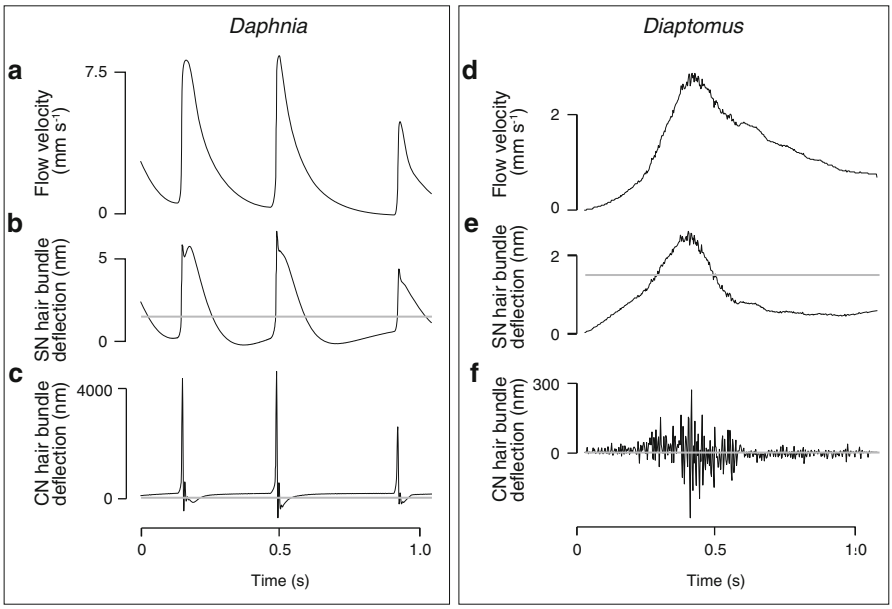

Fig. 5 Detecting the flow created by zooplankton. The flow velocity generated by two species of crustacean was measured by hot-wire anemometry (Montgomery, 1989). For each, we calculated the response of hair bundle deflection to the flow stimulus for both CN and SN biophysical models (Fig. 2) using time-domain filtering (Section 3.1; Fig. 3). The horizontal gray lines illustrate the threshold deflection (Section 2.3) for the SN (**b, e**) and CN (**c**, **f**). According to this calculation, (**a**) the velocity stimulus created by *Daphnia* was detected with high fidelity by (**b**) the SN neuromast. (**c**) In contrast, the CN neuromast responded with a high-intensity deflection to only the most rapid events in the stimulus. (**d–f**) Similar results were predicted for the stimulus generated by *Diaptomus*. (**d**) The flow velocity created by this animal is well reflected by (**e**) the small deflections of the SN, but (**f**) the rapid events are reflected in the large-amplitude response of the CN

CNs and SNs filter these different signals, the responses of both types may be calculated by time-domain filtering (Section 3.1).

Daphnia (Fig. 5a–c) swim with an oscillatory motion at a relatively low frequency and these pulses are interrupted by recovery strokes (Fig. 5). When exposed to this stimulus, the SN hair bundle deflections largely mirror the velocity of this flow pattern (Fig. 5b) with a relatively low amplitude. Therefore, SNs offer good fidelity to the velocity profile of this stimulus. In contrast, CNs accentuate the rapid events in a velocity signal and attenuate relatively slow flows. As a consequence, a CN responds with a high-amplitude deflection to the onset of the power stroke, but shows little response to the recovery stroke of *Daphnia*. The CN response thereby serves as an event marker for the initiation of propulsive cycles, but not a comprehensive reflection of changes in velocity.

The contrast in filtering between a SN and CN is even more dramatic for the stimulus produced by *Diaptomus* (Fig. 5d). The modeled SN response reflects

nearly all features of the velocity of the stimulus (Fig. 5e). However, much of this response is below transducer noise levels and therefore unlikely to be detected by SNs (van Netten et al., 2003; see also Section 2). SNs therefore encode the slow changes in flow as the zooplankton achieves high speeds. In contrast, the CN response filters out this slow change and emphasizes the high-frequency (~50 Hz) oscillations produced by the swimmerets with a far superior signal-to-noise ratio than the SN signal (Fig. 5f). Therefore, the SN and CN responses reflect complementary components of the stimulus produced by *Diaptomus*.

4 Unresolved Questions

Fundamental questions remain about the biophysics of lateral line neuromasts. Although a comprehensive picture is emerging for how CNs filter and encode stimuli, there remains less certainty about SNs. For example, it is not clear whether the hair cells within SNs possess the same filtering properties as in CNs. This uncertainty complicates our understanding for the role of each submodality in behavior (see also the chapter by Chagnaud & Coombs), and behavioral studies largely have yet to determine how SNs and CNs individually influence the behavior of fishes.

4.1 Are the Hair Cells within SNs and CNs Different?

It is increasingly clear how canal neuromasts detect flow stimuli. Biophysical models of the canal and CN cupula can successfully predict the extracellular potentials of the hair cells (Ćurčić-Blake & van Netten, 2006) and the afferent action potentials (Coombs & Janssen, 1990; Kroese & Schellart, 1992; Goulet et al., 2008) for an oscillatory flow stimulus. The dominance of mechanical properties in the CN frequency response is facilitated by the relative broad tuning of its hair cells (Kroese & van Netten, 1989), and there is evidence that in ruffe (*Gymnocephalus cernua*) the low-pass filtering of a CN hair cell exhibits a temperature-dependent cutoff frequency that under normal habitat conditions is tuned to mechanical properties (Wiersinga-Post & van Netten, 2000).

Mechanics may not similarly dictate the frequency response of superficial neuromasts. Studies on SN afferent activity indicate cutoff frequencies for a velocity stimulus on the order of tens of Hertz (Kroese & Schellart, 1992), which is not predicted by biophysical models so far (Fig. 2d). Therefore, the neurophysiology of SN hair cells may attenuate high frequencies in a manner that is not similarly found in CN hair cells. However, this issue remains unresolved because of possible differences between the flow stimulus used in neurophysiological measurements (e.g., Kalmijn, 1988) and that considered by biophysical models (e.g., McHenry et al., 2008).

A difference in the physiological or mechanical properties of hair cells has the potential to affect the limits of sensitivity in SNs and CNs. By neglecting such a difference, the present modeling results suggest that SNs generate relatively small hair bundle displacements as compared to CNs when exposed to the same oscillatory stimulus (e.g., Fig. 4, 5). This result emerges predominantly from the larger dimensions of CNs. In addition, the expected equivalent noise levels of SNs are higher mainly because of the fewer hair cells of SNs (see Münz, 1989, for data; van Netten et al., 2003). Together this results in an overall superior signal-to-noise ratio of hair bundle responses of a single CN as compared to those of a SN (see Section 2.3). This view is supported by threshold measurements of afferent neurons of both SNs and CNs in the mottled sculpin (Coombs & Janssen, 1989). However, it remains possible that SNs could compensate for their fewer numbers of hair cells with higher sensitivity in each hair cell. Also, afferent fibers may enhance the signal component over the noise by contacting many SNs (Münz, 1989) and thereby integrate the responses of hair cells of several cupulae. On the other hand, a less sensitive SN should detect high intensities, where CNs would be saturated. This means that a lower SN sensitivity could provide information about high-amplitude events, assuming a fixed and similar operational displacement range of the hair cells in both types of neuromasts.

The comparison we made is based on results from SNs in zebrafish and the rather large CNs in the ruffe. In other fish species the ratio of absolute hair bundle responses to the same stimulus may differ. Nevertheless, it is to be expected that because of the general morphological differences that govern their biophysical detection properties, SNs respond with smaller hair bundle deflection than those of CNs at higher frequencies, up to hundreds of Hertz (Fig. 2e, f).

4.2 Do CNs and SNs Play Different Roles in Behavior?

Experiments on predatory behavior offer compelling evidence for an integral role of CNs. The ability to detect and localize prey in mottled sculpin is likely limited by the sensitivity and threshold of the lateral line (Coombs & Janssen, 1990). CNs are better suited to this task over the less sensitive SNs (Fig. 2), particularly for the relatively high frequencies generated by the swimming motions of zooplankton (Fig. 5; Section 3). Indeed, this behavior was unaltered by ablating the SNs, but was extinguished by a chemical ablation of the entire system, including CN neuromasts (Coombs et al., 2001). In contrast, SNs appear to play an important role in prey fish. Zebrafish larvae, which lack CNs, require SNs to evade a predator (Stewart et al., 2013). This ability depends on the motion of the body relative to the surrounding water (Stewart et al., 2010) and becomes less sensitive during swimming (Feitl et al., 2010).

The canal lateral line system may offer advantages in detecting stimuli in environments with high currents. When exposed to a constant unidirectional flow, an oscillatory stimulus remains detectable to fibers innervating CNs, but not SNs in

trout (*Oncorhynchus mykiss*) and goldfish (Engelmann et al., 2000, 2002). This result is consistent with the frequency response of CNs, which filters out direct currents more strongly due to the hydrodynamics of the canal (Fig. 2b). Although exhibiting lower sensitivity for a wide range of frequencies (Fig. 2e, f), SNs are apparently saturated by rapid unidirectional flow and consequently become insensitive to an additional oscillatory flow stimulus, such as what might be generated by a prey (Fig. 5).

If not saturated, SNs may enable a fish to detect turbulent flows. In light of recent findings (Van Trump et al., 2010), the results of experiments on trout that combined an aminoglycoside treatment with mechanical ablation may be interpreted as demonstrating that SNs affect the duration of entrained swimming behind obstacles in flow (Montgomery et al., 2003). Consistent with this finding, experiments on goldfish suggest that posterior lateral line afferents shown to respond to vortex rings most likely innervate SNs (Chagnaud et al., 2006). Such flows, and those generated by self-motion and other animals, are characterized by high spectral power for frequencies around 10 Hz (Bleckmann et al., 1991), where SNs exhibit relatively high sensitivity (Fig. 2f; Coombs and Janssen, 1990). Therefore, SNs appear to play a role in behaviors that depend on relatively high-intensity turbulent flows.

Given the sensitivity of SNs to unidirectional flow, one might expect this submodality to play a role in the rheotactic (orienting) behaviors of fish to environmental currents. However, current evidence on this matter is inconclusive. Support has been provided by behavioral experiments that used aminoglycoside antibiotics to differentially ablate neuromasts. These antibiotics create a chemical disturbance of hair cell response by blocking hair cell transduction channels (Kroese et al., 1989; Marcotti et al., 2005; see also the chapter by Coffin et al.). Streptomycin is equally effective in creating this effect in the hair cells of both SNs and CN. However, gentamicin reportedly affected only the hair cells of canal neuromasts (Song et al., 1995). Taking advantage of this effect, behavioral experiments on rheotaxis attempted to differentially ablate SNs and CNs in combination with a mechanical ablation to eliminate only SNs (Montgomery et al., 1997). However, recent studies suggest that gentamicin actually blocks a large percentage of both SNs and CNs (Van Trump et al., 2010). Thus, it is difficult to explain why rheotaxis was affected by streptomycin (intended to block both CNs and SNs) but not gentamicin (intended to selectively block CNs). In support of a role of SNs in rheotaxis, mechanical ablation of SNs on the skin surface significantly reduced the rheotactic response in much the same manner as streptomycin, which blocks both CNs and SNs. Thus, there is some evidence that SNs, but not CNs, are important to rheotaxis, but only at relatively slow flows.

5 Summary

The two submodalities of the fish lateral line system are sensitive to different aspects of a flow stimulus owing to the biophysics of the neuromasts. In SNs, boundary layer hydrodynamics and fluid–structure interaction mechanics combine

to create a sensor that is velocity sensitive with high-pass filtering. The cutoff frequency for this filter is on the order of a few Hertz and varies with the dimensions of the cupula and number of hair cells. CNs are generally at least more than an order of magnitude more sensitive than SNs and respond in proportion to flow acceleration over a wide range of frequencies. They exhibit low-pass filtering with a cutoff frequency in the hundreds of Hertz, which is determined by the size of the cupula and the canal. Therefore, the sensitivity of the two submodalities encompasses distinct regimes of stimulus intensity and frequency.

These differences between the types of neuromast are reflected in their filtered responses in the time domain. SNs are predicted to generate responses with high fidelity to the velocity of many biological stimuli (Fig. 5a, e). CNs exhibit a stronger response (Fig. 5c, f), but preferentially sense high-frequency components. Consistent with this result, CNs appear to be employed in behaviors that are limited by neuromast sensitivity or benefit from their ability to filter out direct currents. In contrast, SNs may aid behaviors that depend on information gleaned from high-intensity flows. Despite these advances, a comprehensive understanding of the respective roles of the two submodalities remains elusive. Investigations that integrate behavioral experiments with neurophysiology and biophysics offer great potential for understanding this distinctive sensory system of fish.

References

Bleckmann, H., Breithaupt, T., Blickhan, R., & Tautz, J. (1991). The time course and frequency content of hydrodynamic events caused by moving fish, frogs, and crustaceans. *Journal of Comparative Physiology A*, 168, 749–757.

Budelmann, B. (1989). Hydrodynamic receptor systems in invertebrates. In S. Coombs, P. Görner, & H. Münz (Eds.), *The mechanosensory lateral line* (pp. 607–631). New York: Springer.

Budelmann, B., & Bleckmann, H. (1988). A lateral line analogue in cephalopods: Water waves generate microphonic potentials in the epidermal head lines of *Sepia* and *Lolliguncula*. *Journal of Comparative Physiology A*, 164, 1–5.

Chagnaud, B. P., Bleckmann, H., & Engelmann, J. (2006). Neural responses of goldfish lateral line afferents to vortex motions. *The Journal of Experimental Biology*, 209, 327–342.

Coombs, S., & Janssen, J. (1989). Peripheral processing by the lateral line of the mottled sculpin (*Cottus bairdi*). In S. Coombs, P. Görner, & H. Münz (Eds.), *The mechanosensory lateral line* (pp. 299–319). New York: Springer.

Coombs, S., & Janssen, J. (1990). Behavioral and neurophysiological assessment of lateral line sensitivity in the mottled sculpin, *Cottus-bairdi*. *Journal of Comparative Physiology A*, 167, 557–567.

Coombs, S., Janssen, J., & Webb, J. F. (1988). Diversity of lateral line systems: Evolutionary and functional considerations. In J. Atema, R. R. Fay, A. N. Popper, & W. N. Tavolga (Eds.), *Sensory biology of aquatic animals* (pp. 553–593). New York: Springer.

Coombs, S., Braun, C. B., & Donovan, B. (2001). The orienting response of Lake Michigan mottled sculpin is mediated by canal neuromasts. *Journal of Experimental Biology*, *204*, 337–348.

Ćurčić-Blake, B., & van Netten, S. (2006). Source location encoding in the fish lateral line canal. *Journal of Experimental Biology*, 209, 1548–1559.

Denton, E. J., & Gray, J. (1983). Mechanical factors in the excitation of clupeid lateral lines. *Proceedings of the Royal Society B: Biological Sciences*, 218, 1–26.

Denton, E. J., & Gray, J. A. B. (1988). Mechanical factors in the excitation of the lateral lines of fishes. In J. Atema, R. R. Fay, A. N. Popper, & W. N. Tavolga (Eds.), *Sensory biology of aquatic animals* (pp. 595–618). New York: Springer.

Denton, E., & Gray, J. (1989). Some observations on the forces acting on neuromasts in fish lateral line canals. In S. Coombs, P. Görner, & H. Münz (Eds.), *The mechanosensory lateral line* (pp. 229–246). New York: Springer.

Dijkgraaf, S. (1963). The functioning and significance of the lateral-line organs. *Biological Reviews*, 38, 51–105.

Dinklo, T. (2005). *Mechano- and electrophysiological studies on cochlear hair cells and superficial lateral line cupulae*. Doctoral dissertation, University of Groningen.

Engelmann, J., Hanke, W., Mogdans, J., & Bleckmann, H. (2000). Neurobiology: Hydrodynamic stimuli and the fish lateral line. *Nature*, 408, 51–52.

Engelmann, J., Hanke, W., & Bleckmann, H. (2002). Lateral line reception in still- and running water. *Journal of Comparative Physiology A,* 188, 513–526.

Feitl, K. E., Ngo, V., & McHenry, M. J. (2010). Are fish less responsive to a flow stimulus when swimming? *The Journal of Experimental Biology*, 213, 3131–3137.

Görner, P. (1963). Untersuchungen zur Morphologie und Elektrophysiologie des Seitenlinienorgans vom Krallenfrosch (*Xenopus laevis* Daudin). *Zeitschrift für vergleichende Physiologie*, 47, 316–338.

Goulet, J., Engelmann, J., Chagnaud, B. P., Franosch, J.-M. P., Suttner, M. D., & Hemmen, J. L. (2008). Object localization through the lateral line system of fish: Theory and experiment. *Journal of Comparative Physiology A*, 194, 1–17.

Goulet, J., van Hemmen, J. L., Jung, S. N., Chagnaud, B. P., Scholze, B., & Engelman, J. (2012). Temporal precision and reliability in the velocity regime of a hair-cell sensory system: The mechanosensory lateral line of goldfish, *Carassius auratus*. *Journal of Neurophysiology*, 107, 2581–2593.

Hudspeth, A. J. (1989). How the ear's works work. *Nature,* 341, 397–404.

Jielof, R., Spoor, A., & de Vries, H. (1952). The microphonic activity of the lateral line. *Journal of Physiology,* 116, 137–157.

Kalmijn, A. J. (1988). Hydrodynamic and acoustic field detection. In J. Atema, R. R. Fay, A. N. Popper, & W. N. Tavolga (Eds.), *Sensory biology of aquatic animals* (pp. 83–130). New York: Springer.

Kalmijn, A. J. (1989). Functional evolution of lateral line and inner ear sensory systems. In S. Coombs, P. Görner, & H. Münz (Eds.), *The mechanosensory lateral line* (pp. 187–215). New York: Springer.

Kramer, G. (1933). Sinnesleistung und das Orientierungsverhalten von *Xenopus laevis*. Zoologische Jahrbücher, *Abteilung für Anatomie und Ontogenie der Tiere*, 52, 629–676.

Kroese, A. B. A., & van Netten, S. M. (1989). Sensory transduction in lateral line hair cells. In S. Coombs, P. Görner, & H. Münz (Eds.), *The mechanosensory lateral line* (pp. 265–284). New York: Springer.

Kroese, A. B. A., & Schellart, N. A. M. (1992). Velocity- and acceleration-sensitive units in the trunk lateral line of trout. *Journal of Neurophysiology*, 68, 2212–2221.

Kroese, A. B. A., van der Zalm, J. M., & van den Bercken, J. (1978). Frequency response of the lateral-line organ of *Xenopus laevis*. *Pfluegers Archiv*, 375, 167–175.

Kroese, A. B. A., Das, A., & Hudspeth, A. J. (1989). Blockage of the transduction channels of hair cells in the bullfrog's sacculus by aminoglycoside antibiotics. *Hearing Research*, 37, 203–217.

Kuiper, J. W. (1956). *The microphonic effect of the lateral line organ*. PhD thesis, University of Groningen, The Netherlands.

Lathi, B. (1998). *Signal processing and linear systems*. New York: Oxford University Press.

Liao, J. C. (2010). Organization and physiology of posterior lateral line afferent neurons in larval zebrafish. *Biology Letters*, 6, 402–405.

Marcotti, W., van Netten, S. M., & Kros, C. (2005). The aminoglycoside antibiotic dihydrostreptomycin rapidly enters mouse outer hair cells through the mechano-electrical transducer channels. *Journal of Physiology,* 567, 505–521.

McHenry, M. J., & van Netten, S. M. (2007). The flexural stiffness of superficial neuromasts in the zebrafish (*Danio rerio*) lateral line. *Journal of Experimental Biology*, 210, 4244–4253.

McHenry, M. J., Strother, J. A., & van Netten, S. M. (2008). Mechanical filtering by the boundary layer and fluid–structure interaction in the superficial neuromast of the fish lateral line system. *Journal of Comparative Physiology A,* 194, 795–810.

McHenry, M. J., Feitl, K. E., Strother, J. A., & Van Trump, W. J. (2009). Larval zebrafish rapidly sense the water flow of a predator's strike. *Biology Letters* 5, 477–497.

Montgomery, J. C. (1989). Lateral line detection of planktonic prey. In S. Coombs, P. Görner, & H. Münz (Eds.), *The mechanosensory lateral line* (pp. 561–574). New York: Springer.

Montgomery, J. C., Baker, C., & Carton, A. (1997). The lateral line can mediate rheotaxis in fish. *Nature,* 389, 960–963.

Montgomery, J. C., McDonald, F., Baker, C. F., Carton, A. G., & Ling, N. (2003). Sensory integration in the hydrodynamic world of rainbow trout. *Proceedings of the Royal Society B: Biological Sciences*, 270, S195–S197.

Münz, H. (1989) Functional organization of the lateral line periphery. In S. Coombs, P. Görner, & H. Münz (Eds.), *The mechanosensory lateral line* (pp. 285–297). New York: Springer.

Schlichting, H. (1979). *Boundary-layer theory*. New York: Springer-Verlag.

Song, J., Yan, H., & Popper, A. (1995). Damage and recovery of hair cells in fish canal (but not superficial) neuromasts after gentamicin exposure. *Hearing Research*, 91, 63–71.

Stewart, W. J., & McHenry, M. J. (2010). Sensing the strike of a predator fish depends on the specific gravity of a prey fish. *The Journal of Experimental Biology*, 213, 3769–3777.

Stewart, W. J., Cardenas, G. S., & McHenry, M. J. (2013) Zebrafish larvae evade predators by sensing water flow. *The Journal of Experimental Biology*, 216, 388–398.

Tsang, P. T. S. K. (1997). *Laser interferometric flow measurements in the lateral line organ*. Doctoral dissertation, University of Groningen.

van Netten, S. M. (1988). Laser interferometer microscope for the measurement of nanometer vibrational displacements of a light-scattering microscopic object. *The Journal of the Acoustical Society of America*, 83, 1667–1674.

van Netten, S. M. (1991). Hydrodynamics of the excitation of the cupula in the fish canal lateral line. *The Journal of the Acoustical Society of America*, 89, 310–319.

van Netten, S. M. (2006). Hydrodynamic detection by cupulae in a lateral line canal: Functional relations between physics and physiology. *Biological Cybernetics*, 94, 67–85.

van Netten, S. M., & Kroese, A. B. A. (1987). Laser interferometric measurements on the dynamic behavior of the cupula in the fish lateral line. *Hearing Research*, 29, 55–62.

van Netten, S. M., Dinklo, T., Marcotti, W., & Kros, C. J. (2003). Channel gating forces govern accuracy of mechano-electrical transduction in hair cells. *Proceedings of the National Academy of Sciences of the USA*, 100, 15510–15515.

Van Trump, W. J., & McHenry, M. J. (2008). The effect of morphological variation on the frequency response of superficial neuromasts in zebrafish (*Danio rerio*). *Journal of Experimental Biology*, 211, 2105–2115.

Watson, G., & Hessinger, D. (1989). Cnidocyte mechanoreceptors are tuned to the movements of swimming prey by chemoreceptors. *Science*, 243, 1589–1591.

Weber, D. D., & Schiewe, M. H. (1976). Morphology and function of the lateral line of juvenile steelhead trout in relation to gas-bubble disease. *Journal of Fish Biology*, 9, 217–233.

Wiersinga-Post, J. E. C., & van Netten, S. M. (2000). Temperature dependency of cupular mechanics and hair cell frequency selectivity in the fish canal lateral line organ, *Journal of Comparative Physiology A*, 186, 949–956.

Wubbels, R. J. (1992). Afferent response of a head canal neuromast of the ruff (*Acerina cernua*) lateral line. *Comparative Biochemistry and Physiology A*, 102, 19–26.